Scission dynamics with K partitions

G. F. Bertsch, W. Younes, and L. M. Robledo

Phys. Rev. C **97**, 064619 — Published 29 June 2018

DOI: 10.1103/PhysRevC.97.064619

Scission Dynamics with K partitions

G.F. Bertsch
Department of Physics and Institute of Nuclear Theory, Box 351560
*University of Washington, Seattle, Washington 98915, USA**

W. Younes
Lawrence Livermore National Laboratory, Livermore, CA 94551, USA †

L.M. Robledo
Center for Computational Simulation, Universidad Politécnica de Madrid,
Campus de Montegancedo, Boadilla del Monte, 28660-Madrid. Spain and
Departamento de Física Teórica, Universidad Autónoma de Madrid, 28049-Madrid, Spain ‡

We propose a framework to calculate the dynamics at the scission point of nuclear fission, based as far as possible on a discrete representation of orthogonal many-body configurations. Assuming axially symmetric scission shapes, we use the K orbital quantum number to build a basis of wave functions. Pre-scission configurations are stable under mean-field dynamics while post-scission configurations evolve to separated fragments. In this first exploratory study, we analyze a typical fission trajectory through to scission in terms of these configurations. We find that there is a major rearrangement of the K occupancy factors at scission. Interestingly, very different fragment shapes occur in the post-scission configurations, even starting from the same pre-scission configuration.

I. INTRODUCTION

The dynamics around the scission point is crucial to understand many aspects of the fission final state, including for example the kinetic energy distribution of the fragments and the odd-even effects in mass distributions. At present [1], the leading tool for microscopic fission theory is the generator coordinate method (GCM) applied to mean-field wave functions derived from energy density functionals. By GCM we understand the whole set of procedures required to carry out the method, from the construction of the set of mean-field wave functions for the generator states, to the calculation of the Hamiltonian overlaps required for both stationary (Hill-Wheeler equation) or dynamic calculations. This has been highly successful to map out the potential energy surface (PES) in a space of nuclear shapes, and to describe the multiple barriers and the topography needed to reproduce the observed excitation functions and mass distributions.

However, the GCM becomes problematic for calculating the dynamics of induced fission. There is a competition between many configurations (collective and non-collective) interacting with each other and the GCM formulation becomes very complicated [5]. Also, the GCM based on shape degrees of freedom hardly has the discrimination power to follow the last state to scission [6]. We will see this very clearly in the example we examine in this article. Finally, there is a computational issue in the GCM associated with the non-orthogonality of the basis functions [3, p. 475].

This has to be contrasted with the theory of spontaneous fission lifetimes. There, a predictive theory is possible using a semi-classical action derived from the PES surface and an inertial tensor also based on the GCM approximations [3–5].

Since the GCM formulation in shape variables turns out to be quite unwieldy, an alternative microscopic fission theory might make use of the configuration-interaction (CI) representation of the many-particle wave function. In contrast to the GCM, which is formulated in terms of continuous generator coordinates, the configuration interaction method diagonalizes a discrete Hamiltonian in the space of Slater determinants. The CI is very well developed for nuclear structure studies [7], but in the fission problem there is the added complication of needing at least some shape degrees of freedom. We would like to use CI methods as far as possible but with deformed mean-field orbitals rather than orbitals from the spherical shell model. Many deformed configurations can be generated as local minima of a Hartree-Fock Hamiltonian. Those configurations do not need any help from a generator coordinate to separate them. And, unlike the GCM configurations, local minima are automatically orthogonal if the single-particle Hamiltonian has some symmetry to classify states by some quantum numbers.

While this approach might diminish the role of the GCM, it can't replace it entirely. In particular, the final state of separated fragments cannot be reasonably represented in a space of local Hartree-Fock (HF) minima, since the final state has no minimum at finite separation.

To explore the feasibility of a CI formalism for fission dynamics, the following questions need to be answered.

Question 1: Can one construct a useful orthogonal basis from the orbitals of self-consistent mean-field theory?

*Electronic address: bertsch@uw.edu
†Electronic address: younes1@llnl.gov
‡Electronic address: luis.robledo@uam.es

Question 2: How do we represent the final state (two fission fragments in the continuum)?

Question 3: How can we calculate the coupling between pre- and post-scission configurations?

In this work, we only address Question 1. We shall examine in detail a typical fission trajectory produced by the GCM using Hartree-Fock-Bogoliubov (HFB) mean-field states. We then project the intermediate wave functions onto a HF basis and examine properties of the states that would go into a CI calculation of the dynamics.

An ultimate goal is to gain a theoretical understanding of the competition between inertial and dissipative dynamics in fission. Statistical models without any dynamic evolution at all have been fairly successful [8, 9]. There are also a number of studies investigating the dynamics in the strongly dissipative limit, e.g. Refs. [10–12]. We also note recent work including both Newtonian inertial dynamics and dissipative effects via Langevin stochastic force [13]. On the other hand, purely quantum Hamiltonian treatments can also exhibit the fluctuations seen in fragment mass distributions [14, 16–18]. So far, there have been few attempts to combine statistical and quantum dynamics in fission, but see Ref. [19]. It should be possible to determine the qualitative character of the dynamics from our present knowledge of the nucleon-nucleon interaction, given a broad enough calculational scheme.

II. THE TRAJECTORY

We model the fission of ^{236}U by following a single trajectory of GCM-constrained HFB configurations. We take the quadrupole operator

$$\hat{Q}_{20} = 2\hat{z}^2 - \hat{x}^2 - \hat{y}^2 \tag{1}$$

as the generator in a HFB calculation of the constrained configurations. Starting from an initial configuration, which could be the ground state, we increase the constrained Q_{20} expectation value by 2 - 4 b, and solve for the new HFB minimum with the previous one as the starting configuration. The energy functional is based on the Gogny D1S interaction [20], with Coulomb exchange treated in the Slater approximation and center-of-mass energy subtracted out of the total kinetic energy. Two codes were used to carry out the HFB minimizations, namely the HFBaxial code by LMR and a similar code by WL [21]. These codes assume that the HFB mean field is axially symmetric, which seems reasonable past the second barrier. Both codes use an axially deformed harmonic oscillator basis; the included h.o. quantum numbers (n_z, n_r, Λ) are selected according to the formula [23]

$$n_z/q + 2n_r + \Lambda \leq N_r \tag{2}$$

with $q = 1.7$ and $n_r = 12$. The codes only treat configurations invariant under time reversal, permitting an additional truncation $\Lambda \geq 0$. The single-particle Hamiltonian is block-diagonal with the largest block ($K = 1/2$) having a dimension of 140. Finally, the h.o. length parameters were fixed at $b_z = 2.97$ fm and $b_r = 1.9$ fm. Often some deformation-dependent optimization is carried out on the length parameters [24], but since our purpose here is largely a qualitative understanding of the configuration space we keep them fixed.

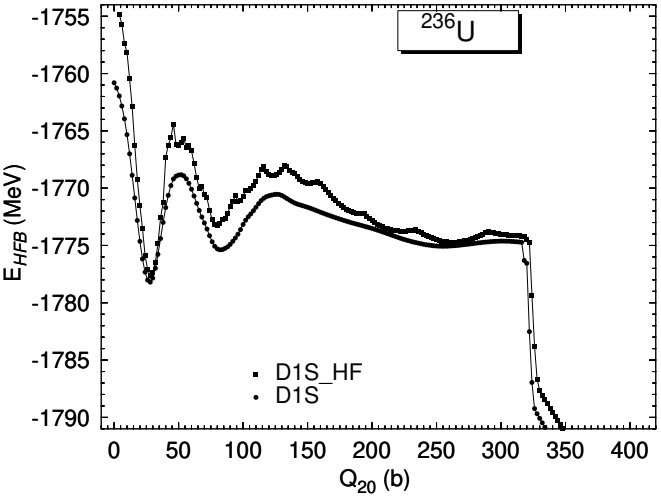

FIG. 1: Solid circles: points on the HFB potential energy surface (PES) constrained by the Q_{20} operator; solid squares: the same PES calculated in the HF approximation as described in Sect. III.

Fig. 1 shows the energy of the GCM states along the computed trajectory. One sees a plateau at high deformation leading to a cliff near $Q_{20} \sim 310$ b. The points beyond that are lower in energy by about 10 MeV. Furthermore, the neck size precipitously drops to a small value [25]. The sudden jump at the cliff edge highlights the problem of understanding scission dynamics. Other measures of the shape are discontinuous as well. Fig. 2 shows the same trajectory in the plane of shape parameters Q_{20} and $Q_{30} = \langle r^3 \sqrt{4\pi/7} Y_{30} \rangle$. One sees that Q_{30} is discontinuous as well. We could try to put in a constraint on Q_{30} to fill in the steps along path, but this turns out to be quite difficult [6]. In a different approach, as many as 5 shape coordinates have been invoked to describe the path to scission [27].

III. HF REDUCTION

By assumption, the HF mean field is axially symmetry and the angular momentum K of the orbitals about the symmetry axis is a good quantum number. Also, we assume that the time-reversed orbitals $\pm K$ are occupied in pairs. Therefore, we can characterize the configurations by the number of pairs of different $|K|$, which we call the *K-partition*. In the absence of an octupole deformation, the particles can be partitioned further by parity, but

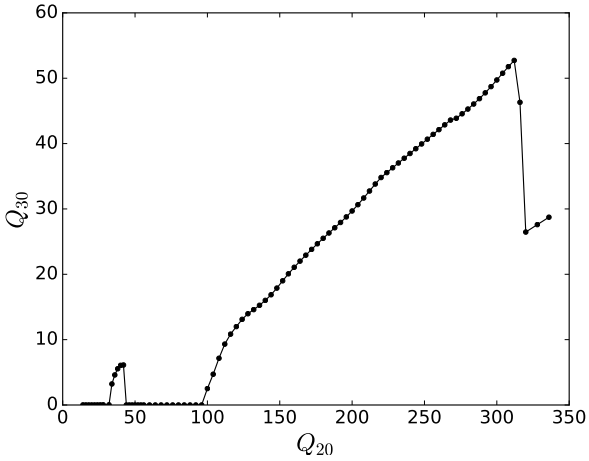

FIG. 2: The PES minima from Fig. 1 in the (Q_{20}, Q_{30}) plane. Lines are shown to guide the eye.

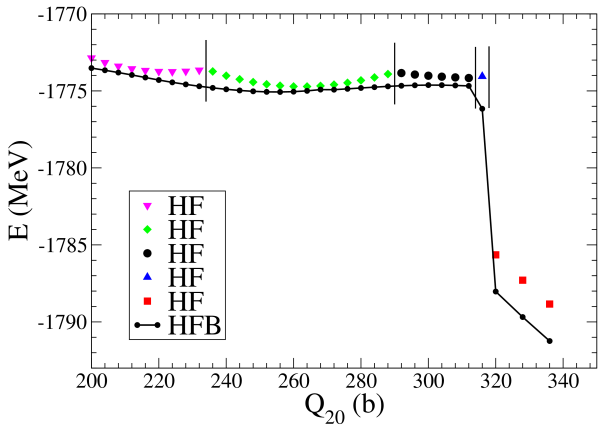

FIG. 3: Expanded view of the constrained minima around the scission point. HF energies for the configurations derived from the HFB path are shown by the symbols in the key, with identical symbols for configurations with the same K-partition. The vertical lines separate the different partitions. The originating HFB energies are shown with the small circles connected by the lines.

that is not possible on the outer fission landscape.

The HFB solutions of course are composed of many HF configurations and we would like to identify the most important ones. One choice to project onto a HF configuration is to adiabatically decrease the strength of the pairing until the wave function approaches a condition where all the orbital occupancy factors are close to zero or one. In the HFBaxial code of LMR, this is achieved by adding to the density constraint an additional one on the particle-number fluctuation. We find that requiring it to be $\langle \hat{N}^2 \rangle - \langle \hat{N} \rangle^2 \sim 0.1$ gives an unambiguous assignment to the HF occupancies. The residual pairing correlation energy under this constraint is less than a tenth of an MeV.

The HF reduction for the HFB states described in the last section is shown in Fig. 1 as the upper curve. The energy difference between the two curves is the pairing correlation energy. Going from ground state to scission, there are about 20 changes of the K-partition along the way. Most of them are recognizable as kinks in the HF PES. From the second barrier on, there are about 9 changes of the K-partition. Fig. 3 shows an expanded view of the two PES's near the scission point, with borders between different K-partitions indicated by vertical lines. The three or four K-partitions near the scission point are of most interest. We give them names as follows: green diamonds, "Lighthouse"; black circles, "Buenavista"; blue triangles, "Glider"; and red squares, "Bobsled".

Note also that the pairing is rather weak in the pre-scission configurations Lighthouse and Buenavista, but it is strong again in Glider and Bobsled. For the remaining discussion, we focus on the properties of the HF-reduced configurations. The densities distributions for the named configurations are shown in Fig. 4. Their K-partitions are listed in Table I. For comparison purposes, we have included the ground state as well in the tabulation. Qualitatively, the major changes are in the $K = 1/2$ orbitals and the high-K orbitals. The higher K becomes depopulated in region where the shape is very elongated. But then Bobsled gains back much of high-K occupancy at the expense of the $K = 1/2$ orbitals. Further aspects of the K-partition distributions near the ground state deformations have been discussed in Ref. [26].

	$2K$ protons						2K neutrons						
Name	1	3	5	7	9	11	1	3	5	7	9	11	13
G.S.	19	13	7	4	2	1	26	19	13	7	4	2	1
Lighthouse	23	13	6	3	1	0	31	20	12	6	2	1	0
Buenavista	23	13	6	3	1	0	32	20	11	6	2	1	0
Glider	22	14	6	3	1	0	31	20	11	6	3	1	0
Bobsled	20	13	7	4	2	0	28	20	12	7	3	2	0

TABLE I: K-partitions for the ground state and some of the configurations close to scission.

Given the K-partitions, we can extend the range of the configurations in shape space by carrying out the HF minimization with both shape and K constraints. The results for the range $Q_{20} = 200 - 350$ b is shown in Fig. 5.

So far, there is no controlled theory for locating where the path jumps from one K-partition to another. To see the ambiguity, let us suppose that the fission path goes through Lighthouse. It could make a big difference in the final state excitation energies (and the total kinetic

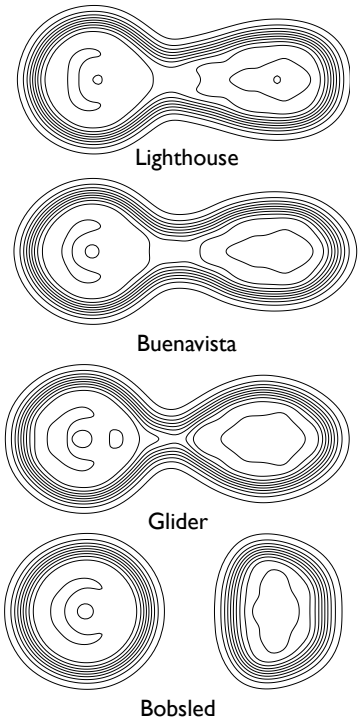

FIG. 4: Density distributions at $Q_{20} = 288, 312, 316$ and 320 b for Lighthouse, Buenavista, Glider and Bobsled, respectively.

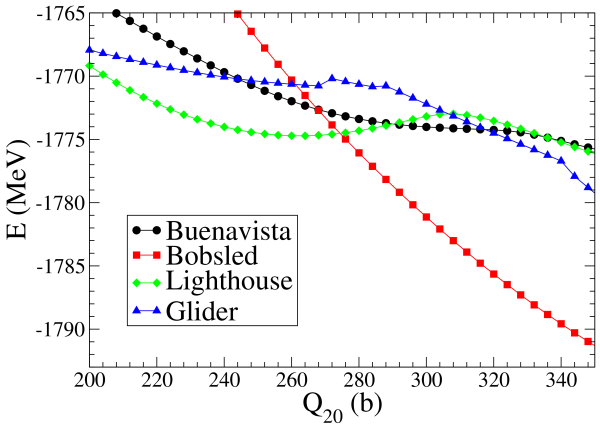

FIG. 5: The PES for the named K-partitions over an extended range of Q_{20}.

energy) whether the jump goes through Bobsled at $Q_{20} \approx 270$ b or through Glider at $Q_{20} \approx 320$ b.

To assess how difficult it is to get from one K-partition to the next along the path, a useful measure is the number of pair jumps in the transition. We define the pair-jump number as

$$N_{J,\sigma} = \tfrac{1}{2} \sum_{K,\sigma} \Delta N_{K,\sigma} \tag{3}$$

with

$$\Delta N_{K,\sigma} = |n_{K,\sigma}(i+1) - n_{K,\sigma}(i)| \tag{4}$$

and $n_{K,\sigma}(i)$ is the number of pairs in orbitals with quantum number K, and $\sigma = n$ or p. The configuration is labeled by i. The total number of jumps is

$$N_J = N_{J,p} + N_{J,n}. \tag{5}$$

Note that the application of the pairing interaction to the wave function induces single pair jumps. Thus, if there are two or more pair jumps the two-particle interaction matrix element between the configurations vanishes.

For the traversal of the fission path from the second saddle to the Glider configuration we find 15 pair jumps. Thus, if the pairing interaction were treated as a perturbation, the endpoint configurations would only be connected in 15th-order perturbation theory. Up until Glider, configuration changes mostly take place by single pair jumps with a few double jumps. One can visualize single jumps as level crossings which become avoided crossing when the pairing interaction is included in the Hamiltonian.

The situation is quite different at the final transition from Glider to Bobsled, which has $N_{J\sigma} = 3$ for both neutrons and protons for a total of $N_J = 6$. There is obviously a major rearrangement at the scission point that would be difficult to describe purely in terms of shape variables.

When there are multiple pair jumps in the transition between HF configurations there will be a number of possible intermediate paths, taking the jumps one by one. For the first jump, there are N_J choices for the starting K, if all the K's are different. The choices for its landing point depends on whether it is a proton or neutron pair; the number of distinct configurations that can be reached by the first proton jump is N_{Jp}^2, provided that all the landing K's are different. For the second and later jump the choices become increasingly restricted until at the penultimate configuration there is only one possibility. The choice of making a neutron or proton jump can also take place in any order. The total number of the minimal-length paths N_P is given by

$$N_P = N_J! \, \frac{N_{Jp}! \, N_{Jn}!}{\Pi_{K\sigma} \Delta N_{K\sigma}!}. \tag{6}$$

According to this formula, there are 2160 minimal-length paths connecting Glider and Bobsled. Many of these paths will be energetically unfavorable and it would be a considerable task to examine them all. As a baseline path, we have examined the HF energies of intermediate steps along the way. Taking the lowest energy landing point at each step starting from glider we obtain the

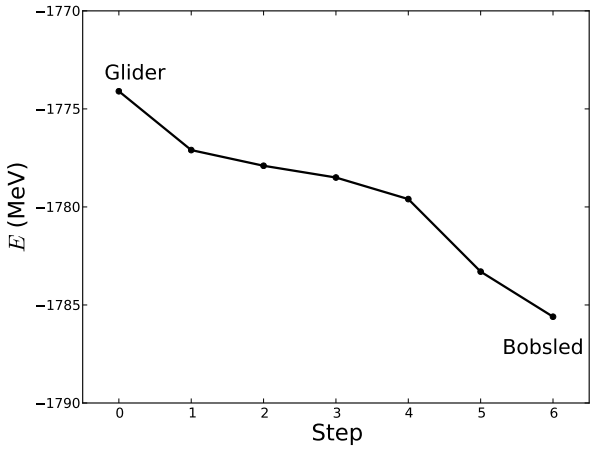

FIG. 6: Intermediate steps from Glider to Bobsled along the minimal-energy path.

path shown in Fig. 6. The energies along the path monotonically decrease, allowing the jump to be accessed by the HFB minimization procedure. The Hamiltonian dynamics would connect the endpoints most effectively if all the configurations along the path have the same energy. If the endpoint has a much lower energy (as is the case here), a quasi-particle excitation of the final configuration at an energy close to the initial energy might be more favored.

IV. HF MINIMA AND POST-SCISSION PROPERTIES

So far we have used both the shape constraints and the K-partition to specify the configuration. Since the shape constraints are continuous quantities, we would like to release them as far as possible to construct a discrete basis. As a first test to exploring their role, we examine how many HF local minima each configuration along the path is attracted to when the shape constraint is removed. Thus we repeat the computation of the minima, starting with the configurations shown in Fig. 5 but without any shape constraint. The K-partition will remain the same under the HF minimization.

Applying this procedure to the named configurations, we find that all configurations with the same K-partition converge to the same state. The converged shape parameters are given in Table II. One sees that the neck parameter is large for Lighthouse, intermediate for Buenavista, and small for Glider and Bobsled. Thus, Lighthouse is a pre-scission configuration, and the last two are post-scission. The finite values of the Q_{20} for Glider and Bobsled is obviously an artifact of the finite dimensional space. Otherwise, the fragments would separate to infinity.

name	Q_{20} (b)	Q_{30} ($b^{3/2}$)	n_{neck}
Lighthouse	262.	42.3	6.9
Buenavista	394.	65.1	1.9
Glider	416.	66.6	0.1
Bobsled	434.	42.9	~ 0.0

TABLE II: Converged shape parameters for the named HF configurations. See [23, 25] for the definition of the neck parameter n_{neck}

When the neck parameter is small, the nucleon numbers and shape parameters of the individual fragments can be determined unambiguously. These parameters are shown in Table III for Glider and Bobsled. Not surprisingly, one of the configurations is anchored by the doubly magic ^{132}Sn. It is interesting to see that the deformation of the light fragment is quite different for the two cases. In one case it is strongly prolate and in the other it is strongly oblate. In fact, the PES in the region of ^{100}Zr has coexisting minima at the two extremes [15], so perhaps it also not surprising that the both can be populated upon scission.

Configuration	fragment	Z	N	Q_{20} (b)
Bobsled	^{132}Sn	50	82	0.4
	^{104}Mo	42	62	-5.3
Glider	^{136}Te	52	84	4.0
	^{100}Zr	40	60	7.6

TABLE III: Fragment properties obtained by releasing the shape constraints for the Bobsled and Glider configuration in Table I.

V. REMAINING QUESTIONS ON EXPLOITING THE CI BASIS

It remains for future work to examine the overlaps between the shape-constrained configurations along the path, as was done in Ref. [28] for the GCM based on an HFB energy functional. If the overlaps are large, one can use some convenient point along the path to represent all of the GCM states there. More likely, the overlaps become too small to ignore at the end points of a K-partition along the path, for example, the states at $Q_{20} = 236$ and 288 b in the Lighthouse configurations. In that case, several states of the same K-partition would be required to span that space along the path. We note that the overlaps can be calculated analytically in the Nilsson harmonic oscillator model [29], but that is too oversimplified for our purposes here.

The localization of particles on the two fragments raises another issue in the construction of the HF basis. For well-separated fragments, the orbitals will be localized on one nucleus or the other except for accidental

degeneracies or fission into identical fragments. Localization to the left or the right can perhaps be used as additional quantum number to specify the HF wave function, playing the same role as the parity of the HF orbitals when the mean field is invariant. No such separation is possible for the highest occupied orbits in the pre-scission configurations. But the possibility of specifying the neutron and proton numbers of the fragments within the HF framework gives an avenue to calculate fluctuations on a finer scale than is possible with only shape degrees of freedom. Even when no clean separation is possible, it may be useful to transform to a orbital basis that maximizes the separation when calculating transition matrix elements between configurations [30]. See also Ref. [31] for a different approach to nucleon localization.

Another issue that needs to be dealt with in the future is the inclusion of states with unpaired particles. In the CI shell-model language, these are the higher seniority states in the generalized seniority wave function basis [32]. It is straightforward to include any configurations of the generalized seniority basis as wave functions in the HF representation. In fact the K-partitions with respect to the nucleons themselves rather than pairs would give more discriminating power. The typical number of unpaired particles ν in the initial compound nucleus for induced fission of ^{236}U by thermal neutrons is large. We can estimate ν by the formula [33]

$$\nu = (aU)^{1/2} \log 4 \tag{7}$$

where a is the usual level density parameter $a \approx A/8$ and U is the back-shifted excitation energy. The result is in the range 15-20. This number changes a lot along the fission path, so we will need estimates of the interaction matrix elements that change the number of quasi-particles, as well as one that are diagonal in quasi-particle number. Obviously, these interaction will have to be treated in some statistical way, perhaps by sampling.

This emphasizes the need to set up a machinery to compute interaction matrix elements between configurations. One difficulty that arises is modeling the nucleon interaction to be employed. As is well known, the energy functionals in use to compute mean-field wave functions are not reliable for residual interactions [34, 35]. Perhaps it might be adequate for the first estimates to use a simple zero-range parameterization of the residual interaction, in the spirit of effective field theories.

VI. PERSPECTIVE

We believe the results presented here are promising to build a useful wave function basis for treating the scission dynamics. We have found two bound configurations at the frontier of the transition, Lighthouse and Buenavista, and two post-fission configurations, Glider and Bobsled. Exactly how the nucleus gets from one configuration to another is far beyond what has been achieved here, but we can see some possible branching of the trajectories. The deformation of the final light fragment is very different in the two post-fission configurations, so the detailed transition dynamics will give a non-trivial prediction for the initial fragment shapes.

It is also of great interest to determine where on the path the transition from the frontier to the HF-unstable configurations takes place. In Fig. 5, Bobsled crosses Lighthouse at $Q_{20} = 274$ b; if the transition took place there, it would not add any internal excitation energy. Thus, the final state would have a relatively large total kinetic energy. On the other hand, if the transition took place at $Q_{20} = 316$ b where the HFB minimization procedure places it, there would need to be a large increase in the number of quasi-particle in the final state to conserve the overall energy. The roughly 10 MeV energy difference between the HFB minima would appear as increased excitation energy in the fragments (and correspondingly lower total kinetic energy).

We look forward to developing this approach along the lines discussed in the previous section to address questions like these.

Acknowledgments

This work was performed under the auspices of the U.S. Department of Energy by Lawrence Livermore National Security, LLC, Lawrence Livermore National Laboratory under Contract DE-AC52-07NA27344. Funding for travel was provided by the U.S. Department of Energy, Office of Science, Office of Nuclear Physics under Contract No. DE-AC02-05CH11231 (LBNL), through the University of California, Berkeley. The work of LMR was partly supported by Spanish MINECO grant Nos. FPA2015-65929 and FIS2015-63770.

[1] N. Schunck and L.M. Robledo, Rep. Prog. Phys. **79** 116301 (2016).
[2] R. Bernard, H. Goutte, D. Gogny, and W. Younes, Phys. Rev. C **84** 044308 (2011).
[3] P. Bonche, J. Dobaczewski, et al., Nucl. Phys. A**510** 466 (1990).
[4] A. Staszczak, A. Baran, et al., Phys. Rev. C **80** 014309 (2009).
[5] R. Rodriguez-Guzman and L.M. Robledo, Phys. Rev. C **89** 054310 (2014).
[6] N. Dubray and D. Regnier, Comp. Phys. Comm. **183** 2035 (2112).
[7] E. Caurier, G. Martinez-Pinedo, et al., Rev. Mod. Phys. **77** 427 (2005).
[8] B.D. Wilkins, E.P. Steinbery and R.R. Chasman, Phys. Rev. C **14** 1832 (1976).

[9] S. Panebianco, J.-L. Sida, et al., Phys. Rev. C **86** 064601 (2012).
[10] Y. Abe, S. Ayik, P.-G. Reinhard and E. Suraud, Phys. Rep. **275** 49 (1996).
[11] J. Randrup and P. Möller, Phys. Rev. Lett. **106** 132503 (2011).
[12] Y. Arimoto and S. Chiba, Phys. Rev. C **88** 044614 (2013).
[13] J. Sadhukhan, C. Zhang, et al., Phys. Rev. C **96** 061301 (2017).
[14] H. Goutte, J.F. Berger, et al., Phys. Rev. C **71** 024316 (2005).
[15] J. Skalski, P.-H. Heenen, and P. Bonche, Nucl. Phys. A **559** 221 (1993).
[16] D. Regnier, N. Dubray, N. Schunck and M. Verrière, Phys. Rev. C **93** 054611 (2016).
[17] H. Tao, J. Zhao, et al., Phys. Rev. C **96** 024319 (2017).
[18] A. Zdeb, A. Dobrowolski, and M. Warda, Phys. Rev. C **95** 054608 (2017).
[19] Y. Tanimura, D. Lacroix, and S. Ayik, Phys. Rev. Lett. **118** 152501 (2017).
[20] J.F. Berger, M. Girod and D. Gogny, Comp. Phys. Comm. **63** 361 (1991).
[21] These codes have been applied to fission in previous publications, eg. [5] and [22].
[22] W. Younes and D. Gogny, Phys. Rev. C **80** 054313 (2009).
[23] M. Warda, J.L. Egido, et al., Phys. Rev. C **66** 014310 (2002).
[24] M. Warda and L. M. Robledo, Phys. Rev. C **84**, 044608 (2011)
[25] Here and in Table II the neck parameters is defined following Ref. [23] as $\hat{n}_{\rm neck} = \exp\left(-(\hat{z}-z_N)^2/a_N^2\right)$ with $a_N = 1$ fm and z_N the position of the neck.
[26] G.F. Bertsch, Int. J. Mod. Phys. E **26** 1740001 (2017).
[27] P. Möller, A. Sierk, et al., Phys. Rev. C **79** 064304 (2009).
[28] M. Verrière, N. Dubray, et al., EPJ Web of Conferences **146** 04034 (2017).
[29] A. Arima and S. Yoshida, Nucl. Phys. **12** 139 (1959).
[30] W. Younes and D. Gogny, Phys. Rev. Lett. **107** 132501 (2011).
[31] C. Zhang, B. Scheutrumpf, and W. Nazarewicz, Phys. Rev. C **94** 064323 (2106).
[32] L.Y. Jia, Phys. Rev. C **96** 034313 (2017).
[33] A. Bohr and B. Mottelson, *Nuclear Structure, Vol. 1*, (Benjamin, New York, 1969), Eq. 2-52.
[34] D. Lacroix, T. Duguet, and M. Bender, Phys. Rev. C **79** 044318 (2009).
[35] L.M. Robledo, J. Phys. G **37** 064020 (2010).